arXiv:1703.05730v1 [hep-ph] 16 Mar 2017

Natural Alignment in the Two Higgs Doublet Model

P. S. Bhupal Dev[1], **Apostolos Pilaftsis**[2]

[1]Department of Physics and McDonnell Center for the Space Sciences, Washington University, St. Louis, MO 63130, USA

[2]Consortium for Fundamental Physics, School of Physics and Astronomy, University of Manchester, Manchester M13 9PL, United Kingdom.

E-mail: bdev@wustl.edu, apostolos.pilaftsis@manchester.ac.uk

Abstract. As the LHC Higgs data persistently suggest the couplings of the observed 125 GeV Higgs boson to be consistent with the Standard Model (SM) expectations, any extended Higgs sector must lead to the so-called SM *alignment limit*, where one of the Higgs bosons behaves exactly like that of the SM. In the context of the Two Higgs Doublet Model (2HDM), this alignment is often associated with either decoupling of the heavy Higgs sector or accidental cancellations in the 2HDM potential. We present a novel symmetry justification for 'natural' alignment without necessarily decoupling or fine-tuning. We show that there exist only *three* different symmetry realizations of the natural alignment scenario in 2HDM. We identify the 2HDM parameter space satisfying the natural alignment condition up to the Planck scale. We also analyze new collider signals for the heavy Higgs sector in the natural alignment limit, which dominantly lead to third-generation quarks in the final state and can serve as a useful observational tool during the Run-II phase of the LHC.

1. Introduction

The discovery of a Higgs boson in the Run-I phase of the LHC [1] provides the first experimental evidence for the Higgs mechanism [2] as the standard theory of electroweak symmetry breaking (EWSB). As more data are being collected at the LHC, the coupling measurements of the observed Higgs boson seem to be very close to the Standard Model (SM) predictions [3]. The constraints deduced from the Higgs signal strength data severely limit the form of a possible heavy scalar sector in the observable sub-TeV range, as predicted by various well-motivated new-physics scenarios, such as supersymmetry.

Here we consider the Two Higgs Doublet Model (2HDM) [4], where the SM Higgs doublet is supplemented by another isodoublet with hypercharge $Y = 1$. In the doublet field space $\Phi_{1,2}$, where $\Phi_i = (\phi_i^+, \phi_i^0)^\mathsf{T}$, the general 2HDM potential reads

$$\begin{aligned} V \;=\; & -\mu_1^2(\Phi_1^\dagger\Phi_1) - \mu_2^2(\Phi_2^\dagger\Phi_2) - \Big[m_{12}^2(\Phi_1^\dagger\Phi_2) + \text{H.c.}\Big] \\ & + \lambda_1(\Phi_1^\dagger\Phi_1)^2 + \lambda_2(\Phi_2^\dagger\Phi_2)^2 + \lambda_3(\Phi_1^\dagger\Phi_1)(\Phi_2^\dagger\Phi_2) + \lambda_4(\Phi_1^\dagger\Phi_2)(\Phi_2^\dagger\Phi_1) \\ & + \left[\frac{\lambda_5}{2}(\Phi_1^\dagger\Phi_2)^2 + \lambda_6(\Phi_1^\dagger\Phi_1)(\Phi_1^\dagger\Phi_2) + \lambda_7(\Phi_1^\dagger\Phi_2)(\Phi_2^\dagger\Phi_2) + \text{H.c.}\right], \end{aligned} \tag{1}$$

which contains *four* real mass parameters $\mu_{1,2}^2$, $\text{Re}(m_{12}^2)$, $\text{Im}(m_{12}^2)$, and *ten* real quartic couplings $\lambda_{1,2,3,4}$, $\text{Re}(\lambda_{5,6,7})$, and $\text{Im}(\lambda_{5,6,7})$. Thus, the vacuum structure of the general 2HDM can be quite rich [5], as compared to the SM.

The quark-sector Yukawa Lagrangian in the general 2HDM is given by

$$-\mathcal{L}_Y^q \;=\; \bar{Q}_L(h_1^d\Phi_1 + h_2^d\Phi_2)d_R \;+\; \bar{Q}_L(h_1^u\widetilde{\Phi}_1 + h_2^u\widetilde{\Phi}_2)u_R \;, \tag{2}$$

where $\widetilde{\Phi}_i = \mathrm{i}\sigma^2\Phi_i^*$ (σ^2 being the second Pauli matrix) are the isospin conjugates of Φ_i, $Q_L = (u_L, d_L)^\mathsf{T}$ are the $SU(2)_L$ quark doublets and u_R, d_R are right-handed quark singlets. To avoid potentially large flavor-changing neutral current processes at the tree level induced by the Yukawa interactions in (2), one imposes a discrete Z_2 symmetry [4] under which

$$\Phi_1 \to -\Phi_1, \quad \Phi_2 \to \Phi_2, \quad u_{Ra} \to u_{Ra}, \quad d_{Ra} \to d_{Ra} \;\text{ or }\; d_{Ra} \to -d_{Ra} \;, \tag{3}$$

($a = 1, 2, 3$ being the quark family index) so that only Φ_2 gives mass to up-type quarks, and only Φ_1 or only Φ_2 gives mass to down-type quarks. The Z_2 symmetry (3) is satisfied by four discrete choices of tree-level Yukawa couplings between the Higgs doublets and SM fermions, which are known as the Type I, II, X (lepton-specific) and Y (flipped) 2HDMs [4]. Global fits to the LHC Higgs data (see e.g., [6, 7]) suggest that all four types of 2HDMs with natural flavor conservation are constrained to lie close to the so-called SM *alignment limit* [8–12], where the mass eigenbasis of the CP-even scalar sector aligns with the SM gauge eigenbasis.

The SM alignment is often associated with the decoupling limit, in which all the non-standard Higgs bosons are assumed to be much heavier than the electroweak scale so that the lightest CP-even scalar behaves just like the SM Higgs boson. The alignment limit can also be achieved, without decoupling [9, 10, 13], but for small $\tan\beta$ values, this is usually attributed to accidental cancellations in the 2HDM potential. We present a novel symmetry argument to naturally justify the alignment limit [11], independently of the kinematic parameters of the theory, such as the heavy Higgs mass and $\tan\beta$. In particular, we show that there exist only *three* possible symmetry realizations of the scalar potential which predict natural alignment. A striking outcome of this analysis is that the heavy Higgs sector is predicted to be *quasi-degenerate*, apart from being *gaugephobic*, which is a generic feature in the alignment limit. Moreover, the current experimental constraints force the heavy Higgs sector to lie above the top-quark threshold. Thus, the dominant collider signal for this sector involves final states with third-generation quarks. We make a detailed study of some of these signals, which can be useful for the heavy Higgs searches in the ongoing Run-II phase of the LHC.

2. Natural Alignment Condition

For simplicity, we consider the CP-conserving 2HDM, but our results can be easily generalized to the CP-violating case. After EWSB by the vacuum expectation values (VEVs) $v_{1,2}$ of the two scalar fields $\Phi_{1,2}$, there are five physical scalar mass eigenstates: two CP-even (h, H), one CP-odd (a) and two charged $(h^\pm)$ scalars. The corresponding mass eigenvalues are given by [14]

$$M_{h^\pm}^2 \;=\; \frac{m_{12}^2}{s_\beta c_\beta} - \frac{v^2}{2}(\lambda_4+\lambda_5) + \frac{v^2}{2s_\beta c_\beta}\left(\lambda_6 c_\beta^2 + \lambda_7 s_\beta^2\right), \qquad M_a^2 \;=\; M_{h^\pm}^2 + \frac{v^2}{2}(\lambda_4-\lambda_5), \tag{4a}$$

$$M_H^2 \;=\; \frac{1}{2}\left[(A+B) - \sqrt{(A-B)^2+4C^2}\right], \qquad M_h^2 \;=\; \frac{1}{2}\left[(A+B) + \sqrt{(A-B)^2+4C^2}\right], \tag{4b}$$

where we have used the short-hand notations $c_\beta \equiv \cos\beta$ and $s_\beta \equiv \sin\beta$ with $\tan\beta = v_2/v_1$ and

$$A \;=\; M_a^2 s_\beta^2 + v^2\left(2\lambda_1 c_\beta^2 + \lambda_5 s_\beta^2 + 2\lambda_6 s_\beta c_\beta\right), \tag{5a}$$

$$B \;=\; M_a^2 c_\beta^2 + v^2\left(2\lambda_2 s_\beta^2 + \lambda_5 c_\beta^2 + 2\lambda_7 s_\beta c_\beta\right), \tag{5b}$$

$$C \;=\; -M_a^2 s_\beta c_\beta + v^2\left(\lambda_{34} s_\beta c_\beta + \lambda_6 c_\beta^2 + \lambda_7 s_\beta^2\right). \tag{5c}$$

with $\lambda_{34} = \lambda_3 + \lambda_4$. The mixing between the mass eigenstates in the CP-odd and charged sectors is governed by the angle β, whereas in the CP-even sector, it is governed by the angle $\alpha = (1/2)\tan^{-1}[2C/(A-B)]$. The SM Higgs field can be identified as the linear combination

$$H_{\rm SM} \;=\; H\cos(\beta-\alpha) + h\sin(\beta-\alpha)\;. \tag{6}$$

Thus, the couplings of h and H to the SM gauge bosons $V = W^\pm, Z$ with respect to the SM Higgs couplings $g_{H_{\rm SM}VV}$ will be respectively $\sin(\beta-\alpha)$ and $\cos(\beta-\alpha)$. The *SM alignment limit* is defined as $\alpha \to \beta$ (or $\alpha \to \beta - \pi/2$) when H (h) couples to vector bosons exactly as in the SM, whereas h (H) becomes *gaugephobic*. For concreteness, we will take the alignment limit as $\alpha \to \beta$.

To derive the alignment condition, we rewrite the CP-even scalar mass matrix as

$$M_S^2 \;=\; \begin{pmatrix} A & C \\ C & B \end{pmatrix} \;=\; \begin{pmatrix} c_\beta & -s_\beta \\ s_\beta & c_\beta \end{pmatrix} \begin{pmatrix} \widehat{A} & \widehat{C} \\ \widehat{C} & \widehat{B} \end{pmatrix} \begin{pmatrix} c_\beta & s_\beta \\ -s_\beta & c_\beta \end{pmatrix}\;, \tag{7}$$

$$\begin{aligned} \text{where}\quad \widehat{A} \;&=\; 2v^2\Big[c_\beta^4\lambda_1 + s_\beta^2 c_\beta^2\lambda_{345} + s_\beta^4\lambda_2 \;+\; 2s_\beta c_\beta\Big(c_\beta^2\lambda_6 + s_\beta^2\lambda_7\Big)\Big]\;, \\ \widehat{B} \;&=\; M_a^2 \;+\; \lambda_5 v^2 \;+\; 2v^2\Big[s_\beta^2 c_\beta^2\Big(\lambda_1+\lambda_2-\lambda_{345}\Big) \;-\; s_\beta c_\beta\Big(c_\beta^2 - s_\beta^2\Big)\Big(\lambda_6-\lambda_7\Big)\Big]\;, \\ \widehat{C} \;&=\; v^2\Big[s_\beta^3 c_\beta\Big(2\lambda_2-\lambda_{345}\Big) - c_\beta^3 s_\beta\Big(2\lambda_1-\lambda_{345}\Big) + c_\beta^2\Big(1-4s_\beta^2\Big)\lambda_6 + s_\beta^2\Big(4c_\beta^2-1\Big)\lambda_7\Big], \end{aligned} \tag{8}$$

and we have used the short-hand notation $\lambda_{345} \equiv \lambda_3 + \lambda_4 + \lambda_5$. Evidently, the SM alignment limit $\alpha \to \beta$ is obtained when $\widehat{C} = 0$ in (7) [9]. This yields the quartic equation

$$\lambda_7\tan^4\beta - (2\lambda_2 - \lambda_{345})\tan^3\beta + 3(\lambda_6-\lambda_7)\tan^2\beta + (2\lambda_1-\lambda_{345})\tan\beta - \lambda_6 \;=\; 0\;. \tag{9}$$

For *natural* alignment, (9) should be satisfied for *any* value of $\tan\beta$, which requires the coefficients of the polynomial in $\tan\beta$ to vanish identically [11]. This implies

$$2\lambda_1 \;=\; 2\lambda_2 \;=\; \lambda_{345}\;, \qquad \lambda_6 \;=\; \lambda_7 \;=\; 0\;. \tag{10}$$

In particular, for $\lambda_6 = \lambda_7 = 0$ as in the Z_2-symmetric 2HDMs, (9) has a solution

$$\tan^2\beta \;=\; \frac{2\lambda_1 - \lambda_{345}}{2\lambda_2 - \lambda_{345}} \;>\; 0\;, \tag{11}$$

independent of M_a. After some algebra, the simple solution (11) to our *natural alignment condition* (9) can be shown to be equivalent to that derived in [10].

3. Symmetry Classifications of the 2HDM Potential

To identify all accidental symmetries of the 2HDM potential (1), it is convenient to work in the *bilinear scalar field formalism* [15] by introducing an 8-dimensional complex multiplet $\mathbf{\Phi} \equiv (\Phi_1, \Phi_2, \widetilde{\Phi}_1, \widetilde{\Phi}_2)^\mathsf{T}$ [5, 16, 17]. In terms of the $\mathbf{\Phi}$-multiplet, we define a *null* 6-dimensional Lorentz vector $R^A \equiv \mathbf{\Phi}^\dagger\Sigma^A\mathbf{\Phi}$, where $A = 0, 1, ..., 5$ and the six 8×8-dimensional matrices Σ^A may be expressed in terms of the three Pauli matrices $\sigma^{1,2,3}$ and the identity matrix $\mathbf{1}_{2\times 2} \equiv \sigma^0$, as follows:

$$\begin{aligned} \Sigma^{0,1,3} \;&=\; \frac{1}{2}\sigma^0\otimes\sigma^{0,1,3}\otimes\sigma^0, \qquad \Sigma^2 \;=\; \frac{1}{2}\sigma^3\otimes\sigma^2\otimes\sigma^0, \\ \Sigma^4 \;&=\; -\frac{1}{2}\sigma^2\otimes\sigma^2\otimes\sigma^0, \qquad \Sigma^5 \;=\; -\frac{1}{2}\sigma^1\otimes\sigma^2\otimes\sigma^0. \end{aligned} \tag{12}$$

symmetry	μ_1^2	μ_2^2	m_{12}^2	λ_1	λ_2	λ_3	λ_4	$\mathrm{Re}(\lambda_5)$	$\lambda_6 = \lambda_7$
$Z_2 \times O(2)$	-	-	Real	-	-	-	-	-	Real
$(Z_2)^2 \times SO(2)$	-	-	0	-	-	-	-	-	0
$(Z_2)^3 \times O(2)$	-	μ_1^2	0	-	λ_1	-	-	-	0
$O(2) \times O(2)$	-	-	0	-	-	-	-	0	0
$Z_2 \times [O(2)]^2$	-	μ_1^2	0	-	λ_1	-	-	$2\lambda_1 - \lambda_{34}$	0
$O(3) \times O(2)$	-	μ_1^2	0	-	λ_1	-	$2\lambda_1 - \lambda_3$	0	0
$SO(3)$	-	-	Real	-	-	-	-	λ_4	Real
$Z_2 \times O(3)$	-	μ_1^2	Real	-	λ_1	-	-	λ_4	Real
$(Z_2)^2 \times SO(3)$	-	μ_1^2	0	-	λ_1	-	-	$\pm\lambda_4$	0
$O(2) \times O(3)$	-	μ_1^2	0	-	λ_1	$2\lambda_1$	-	0	0
$SO(4)$	-	-	0	-	-	-	0	0	0
$Z_2 \times O(4)$	-	μ_1^2	0	-	λ_1	-	0	0	0
$SO(5)$	-	μ_1^2	0	-	λ_1	$2\lambda_1$	0	0	0

Table 1: Relations between the parameters of the $U(1)_Y$-invariant 2HDM potential (1) for the 13 accidental symmetries [17] in a diagonally reduced basis, where $\mathrm{Im}(\lambda_5) = 0$ and $\lambda_6 = \lambda_7$. The symmetries in blue satisfy the natural alignment condition (10).

Note that the bilinear field space spanned by the 6-vector R^A realizes an *orthochronous* $SO(1,5)$ symmetry group [5,17].

In terms of the null-vector R^A, the 2HDM potential (1) takes on a simple quadratic form:

$$V \;=\; -\frac{1}{2}\, M_A\, R^A \;+\; \frac{1}{4}\, L_{AB}\, R^A R^B \;, \tag{13}$$

where M_A and L_{AB} are $SO(1,5)$ constant 'tensors' that depend on the mass parameters and quartic couplings given in (1) and their explicit forms may be found in [17,18]. Requiring that the $SU(2)_L$ gauge-kinetic term of the $\mathbf{\Phi}$-multiplet remains canonical restricts the allowed set of rotations from SO(1,5) to SO(5), where only the spatial components R^I (with $I = 1, ..., 5$) transform and the zeroth component R^0 remains invariant. Consequently, in the absence of the hypercharge gauge coupling and fermion Yukawa couplings, the maximal symmetry group of the 2HDM is $G^R_{\mathrm{2HDM}} = SO(5)$. Including all proper, improper and semi-simple subgroups of SO(5), the accidental symmetries for the 2HDM potential were completely classified in [5,17], as shown in Table 1. Here we have used a diagonally reduced basis [19], where $\mathrm{Im}(\lambda_5) = 0$ and $\lambda_6 = \lambda_7$, thus reducing the number of independent quartic couplings to seven. Each of the symmetries listed in Table 1 leads to certain constraints on the mass and/or coupling parameters. From Table 1, we find that there are *only* three symmetries, namely $Z_2 \times [O(2)]^2$, $O(3) \times O(2)$, and SO(5), which satisfy the natural alignment condition given by (10).[1] In the next two sections, we analyze each of these three realizations of the SM alignment. The simplest case based on the SO(5) group has already been discussed in details in Refs. [11,23]. Our preliminary results reported for the other two cases are taken from our upcoming publication [24].

[1] In Type-I 2HDM, there exists an additional possibility of realizing an exact Z_2 symmetry [20] which leads to an exact alignment, i.e. in the context of the so-called inert 2HDM [21]. In general, for nHDM with $m < n$ inert scalar doublets, there are still three continuous alignment symmetries in the field space of the non-inert sector [22].

4. Maximally Symmetric 2HDM

From Table 1, we see that the maximal symmetry group in the bilinear field space is SO(5), in which case the parameters of the 2HDM potential (1) satisfy the following relations:

$$\begin{aligned} &\mu_1^2 \;=\; \mu_2^2\,, \quad m_{12}^2 \;=\; 0\,, \\ &\lambda_2 \;=\; \lambda_1\,, \quad \lambda_3 \;=\; 2\lambda_1\,, \quad \lambda_4 \;=\; \mathrm{Re}(\lambda_5) \;=\; \lambda_6 \;=\; \lambda_7 \;=\; 0\,, \end{aligned} \tag{14}$$

Thus, the 2HDM potential (1) is parameterized by just a *single* mass parameter $\mu_1^2 = \mu_2^2 \equiv \mu^2$ and a *single* quartic coupling $\lambda_1 = \lambda_2 = \lambda_3/2 \equiv \lambda$, as in the SM:

$$V \;=\; -\,\mu^2\left(|\Phi_1|^2 + |\Phi_2|^2\right) \;+\; \lambda\left(|\Phi_1|^2 + |\Phi_2|^2\right)^2 \;=\; -\,\frac{\mu^2}{2}\,\mathbf{\Phi}^\dagger\,\mathbf{\Phi} \;+\; \frac{\lambda}{4}\left(\mathbf{\Phi}^\dagger\,\mathbf{\Phi}\right)^2\,. \tag{15}$$

Given the isomorphism of the Lie algebras SO(5) $\sim$ Sp(4), the maximal symmetry group of the 2HDM in the original $\mathbf{\Phi}$-field space is $\mathrm{G}_{\mathrm{2HDM}}^{\mathbf{\Phi}} = [\mathrm{Sp}(4)/\mathrm{Z}_2] \times \mathrm{SU}(2)_L$ [11, 17] in the custodial symmetry limit of vanishing g' and fermion Yukawa couplings.

4.1. Scalar Spectrum

Using the parameter relations given by (14), we find from (4a) and (4b) that in the MS-2HDM, the CP-even scalar H has mass $M_H^2 = 2\lambda_2 v^2$, whilst the remaining four scalar fields, denoted hereafter as h, a and $h^\pm$, are massless. This is a consequence of the Goldstone theorem, since after electroweak symmetry breaking, SO(5) $\xrightarrow{\langle\Phi_{1,2}\rangle\neq 0}$ SO(4). Thus, we identify H as the SM-like Higgs boson with the mixing angle $\alpha = \beta$ [cf. (6)], i.e. the SM alignment limit can be naturally attributed to the SO(5) symmetry of the theory.

In the exact SO(5)-symmetric limit, the scalar spectrum of the MS-2HDM is experimentally unacceptable. This is because the four massless pseudo-Goldstone particles, viz. h, a and $h^\pm$, have sizeable couplings to the SM Z and $W^\pm$ bosons, and could induce additional decay channels, such as $Z \to ha$ and $W^\pm \to h^\pm h$, which are experimentally excluded [30]. However, as we will see below, the SO(5) symmetry may be violated predominantly by RG effects due to g' and third-generation Yukawa couplings, as well as by soft SO(5)-breaking mass parameters, thereby lifting the masses of these pseudo-Goldstone particles to be consistent with the experimental constraints.

4.2. RG and Soft Breaking Effects

To calculate the RG and soft-breaking effects in a technically natural manner, we assume that the SO(5) symmetry is realized at some high scale μ_X much above the electroweak scale. The physical mass spectrum at the electroweak scale is then obtained by the RG evolution of the 2HDM parameters given by (1). Using the two-loop RG equations (RGEs) given in Ref. [11], we first examine the deviation of the Higgs spectrum from the SO(5)-symmetric limit due to g' and Yukawa coupling effects, in the absence of the soft-breaking term. This is illustrated in Figure 1 for a typical choice of parameters in the Type-II realization of the 2HDM. We find that the RG-induced g' effects only lift the charged Higgs mass $M_{h^\pm}$, while the corresponding Yukawa coupling effects also lift slightly the mass of the non-SM CP-even pseudo-Goldstone boson h. However, they still leave the CP-odd scalar a massless, which can be identified as a $\mathrm{U}(1)_{\mathrm{PQ}}$ axion [31].

Therefore, g' and Yukawa coupling effects are *not* sufficient to yield a viable Higgs spectrum at the weak scale, starting from a SO(5)-invariant boundary condition (14) at some high scale μ_X. To minimally circumvent this problem, we include soft SO(5)-breaking effects, by assuming a non-zero soft-breaking term $\mathrm{Re}(m_{12}^2)$. In the SO(5)-symmetric limit for the scalar quartic

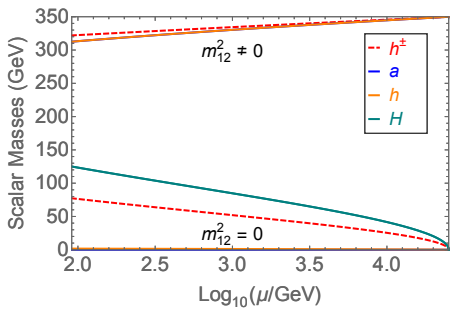

Figure 1: The scalar spectrum in the MS-2HDM without and with soft-breaking effects.

couplings, but with $\mathrm{Re}(m_{12}^2) \neq 0$, we obtain the following mass spectrum [cf. (4a) and (4b)]:

$$M_H^2 \;=\; 2\lambda_2 v^2 \;, \qquad M_h^2 \;=\; M_a^2 \;=\; M_{h^\pm}^2 \;=\; \frac{\mathrm{Re}(m_{12}^2)}{s_\beta c_\beta} \;, \tag{16}$$

as well as an equality between the CP-even and CP-odd mixing angles: $\alpha = \beta$, thus predicting an *exact* alignment for the SM-like Higgs boson H, simultaneously with an experimentally allowed heavy Higgs spectra (cf. Figure 1 for $m_{12}^2 \neq 0$ case). Note that in the alignment limit, the heavy Higgs sector is exactly degenerate [cf. (16)] at the SO(5) symmetry-breaking scale, and at the low-energy scale, this degeneracy is mildly broken by the RG effects. Thus, we obtain a *quasi-degenerate* heavy Higgs spectrum, which is a unique prediction of the MS-2HDM, valid even in the non-decoupling limit, and can be used to distinguish this model from other 2HDM scenarios.

4.3. Misalignment Predictions

As discussed in Section 4.2, there will be some deviation from the alignment limit in the low-energy Higgs spectrum of the MS-2HDM due to RG and soft-breaking effects. By requiring that the mass and couplings of the SM-like Higgs boson H are consistent with the LHC Higgs data [3], we derive predictions for the remaining scalar spectrum and compare them with the existing (in)direct limits on the heavy Higgs sector. We use the constraints in the $(\tan\beta,\ \beta-\alpha)$ plane derived from a recent global fit for the Type-II 2HDM [32], and require that for a given set of SO(5) boundary conditions $\{\mu_X, \tan\beta(\mu_X), \lambda(\mu_X)\}$, the RG-evolved 2HDM parameters at the weak scale must satisfy these alignment constraints on the lightest CP-even Higgs boson sector. This puts stringent constraints on the MS-2HDM parameter space, as shown in Figure 2 by the blue shaded region. In the red shaded region, there is no viable solution to the RGEs. We ensure that the remaining allowed (white) region satisfies the necessary theoretical constraints, i.e. positivity and vacuum stability of the Higgs potential, and perturbativity of the Higgs self-couplings [4]. From Figure 2, we find that there exists an *upper* limit of $\mu_X \lesssim 10^9$ GeV on the SO(5)-breaking scale of the 2HDM potential, beyond which an ultraviolet completion of the theory must be invoked. The situation can be alleviated with the other two natural alignment scenarios listed in Table 1 and this will be the subject of the next section.

For the allowed parameter space of our MS-2HDM as shown in Figure 2, we obtain concrete predictions for the remaining Higgs spectrum. In particular, the alignment condition imposes a *lower* bound on the soft breaking parameter $\mathrm{Re}(m_{12}^2)$, and hence, on the heavy Higgs spectrum. A comparison of the global fit limit on the charged Higgs-boson mass as a function of $\tan\beta$ [32] with our predicted limits from the alignment condition in the MS-2HDM for a typical value of the boundary scale $\mu_X = 3 \times 10^4$ GeV is shown in Figure 3 (left panel). It is clear that the alignment limits are stronger than the global fit limits, except in the very small and very large $\tan\beta$ regimes.

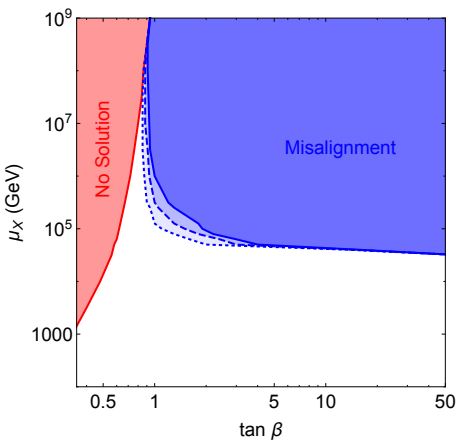

Figure 2: The 1σ (dotted), 2σ (dashed) and 3σ (solid) exclusion contours (blue shaded region) from the alignment constraints in MS-2HDM. The red shaded region is theoretically excluded.

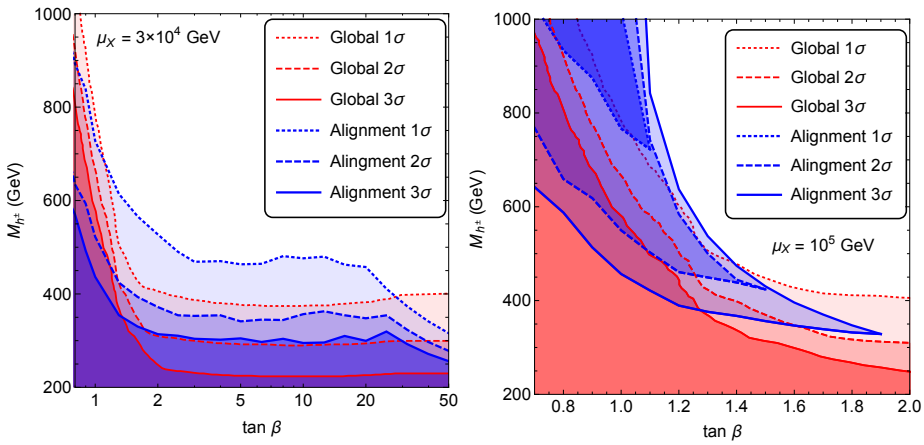

Figure 3: *Left:* The 1σ (dotted), 2σ (dashed) and 3σ (solid) *lower* limits on the charged Higgs mass obtained from the alignment condition (blue lines) in the MS-2HDM with $\mu_X = 3 \times 10^4$ GeV. *Right:* The 1σ (dotted), 2σ (dashed) and 3σ (solid) *allowed* regions from the alignment condition (blue lines) for $\mu_X = 10^5$ GeV. For comparison, the corresponding lower limits from a global fit are also shown (red lines).

From Figure 2, we note that for $\mu_X \gtrsim 10^5$ GeV, phenomenologically acceptable alignment is not possible in the MS-2HDM for large $\tan\beta$ *and* large m_{12}^2. Therefore, we also get an *upper* bound on the charged Higgs-boson mass $M_{h^\pm}$ from the misalignment condition, depending on $\tan\beta$. This is illustrated in Figure 3 (right panel) for $\mu_X = 10^5$ GeV.

Similar alignment constraints are obtained for the heavy neutral pseudo-Goldstone bosons h and a, which are predicted to be quasi-degenerate with the charged Higgs boson $h^\pm$ in the MS-2HDM [cf. (16)]. The current experimental limits on the heavy neutral Higgs sector [30] are weaker than the alignment constraints in this case. Thus, the MS-2HDM scenario provides a natural reason for the absence of a heavy Higgs signal below the top-quark threshold, and this has important consequences for the heavy Higgs searches in the Run-II phase of the LHC, as discussed in Sec. 6.

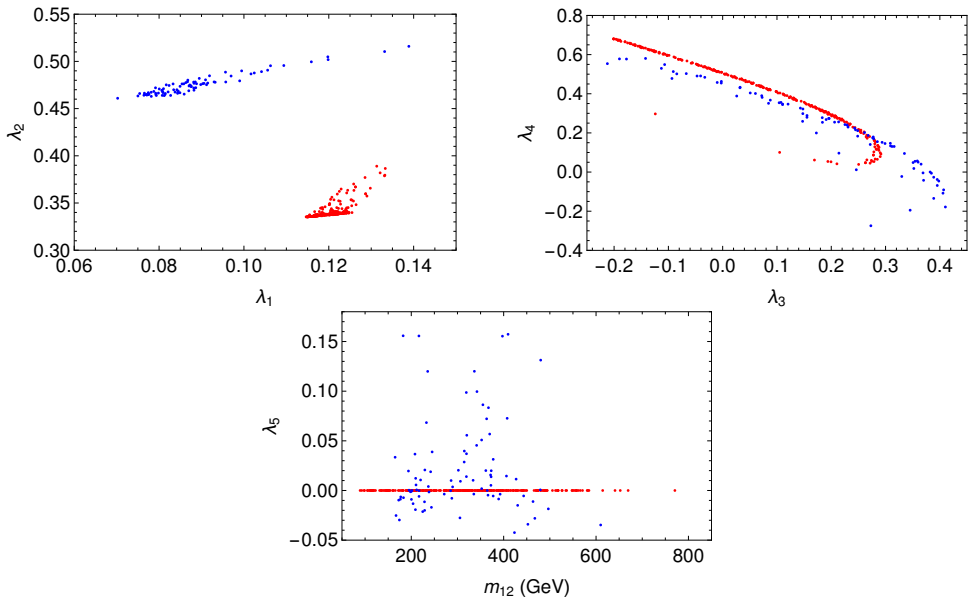

Figure 4: The 2HDM parameter space at the EW scale satisfying the natural alignment condition up to the Planck scale. The red points are for the $\mathrm{O}(3) \times \mathrm{O}(2)$ case and the blue points are for the $\mathrm{Z}_2 \times [\mathrm{O}(2)]^2$ case. We have shown the results for the $\tan\beta = 2$ case.

5. Planck-scale Perturbative Next-to-maximally Symmetric 2HDM

As discussed in Section , the MS-2HDM scenario cannot be realized beyond $\mu_X \gtrsim 10^9$ GeV. However, as we show in this section, the other two natural alignment scenarios discussed in Table 1, namely, those based on the $\mathrm{Z}_2 \times [\mathrm{O}(2)]^2$ and $\mathrm{O}(3) \times \mathrm{O}(2)$ symmetry of the 2HDM potential, can be realized all the way up to the Planck scale, assuming no other intermediate new physics scale. To see this, we choose $\mu_X = M_{\mathrm{Pl}} = 1.2 \times 10^{19}$ GeV and apply the boundary conditions given in Table 1 for these two cases. For the $\mathrm{Z}_2 \times [\mathrm{O}(2)]^2$ symmetry, this leaves three quartic couplings free, namely, $\lambda_{1,3,4}$, whereas for the $\mathrm{O}(3) \times \mathrm{O}(2)$ case, only two are free, namely, $\lambda_{1,3}$. We also allow for a non-zero m_{12}^2 to get a realistic scalar mass spectrum. Using the one-loop RGEs given in Ref. [11], we then study the top-down evolution of the 2HDM parameter space up to the weak scale and examine those points satisfying the vacuum stability, perturbativity and the LHC Higgs data, including the SM Higgs mass and the alignment constraints. Our numerical results are given in Figure 4 for the $\lambda_1 - \lambda_2$, $\lambda_3 - \lambda_4$, and $\lambda_5 - m_{12}$ parameter space at the weak scale, respectively. We have shown the results for the $\tan\beta = 2$ case, and the corresponding results for higher t_β values can be found in Ref. [24].

The corresponding scalar mass spectra are shown in Figure 5, where in the x-axis, we have plotted the heavy neutral Higgs mass $m_h \simeq m_a$ and on the y-axis, the charged Higgs mass $m_{h^\pm}$. It is clear that as in the MS-2HDM case, the heavy Higgs spectrum is quasi-degenerate. Thus, we conclude that the near-degeneracy of the heavy Higgs spectrum is a generic prediction of the natural alignment scenario, irrespective of the underlying symmetry of the 2HDM potential. This is a key result that will be important for the collider signal analysis in the next section.

6. Collider Signatures in the Alignment Limit

In the alignment limit, the couplings of the lightest CP-even Higgs boson are exactly similar to the SM Higgs couplings, while the heavy CP-even Higgs boson is gaugephobic. Therefore, two of the relevant Higgs production mechanisms at the LHC, namely, the vector boson fusion and Higgsstrahlung processes are suppressed for the heavy neutral Higgs sector. As a consequence,

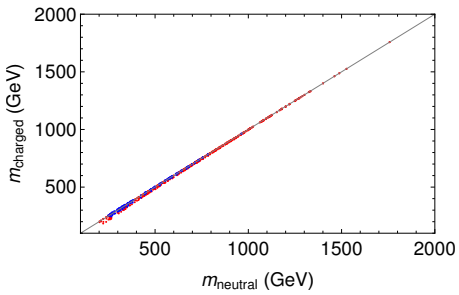

Figure 5: The scalar mass spectrum at the EW scale satisfying the natural alignment condition up to the Planck scale. The red points are for the $\mathrm{O}(3) \times \mathrm{O}(2)$ case and the blue points are for the $\mathrm{Z}_2 \times [\mathrm{O}(2)]^2$ case. The gray line shows the exact degeneracy. We have shown the results for the $\tan\beta = 2$ case.

the only relevant production channels to probe the neutral Higgs sector of the MS-2HDM are the gluon-gluon fusion and $t\bar{t}h$ ($b\bar{b}h$) associated production mechanisms at low (high) $\tan\beta$. For the charged Higgs sector of the MS-2HDM, the dominant production mode is the associated production process: $gg \to \bar{t}bh^+ + t\bar{b}h^-$, irrespective of $\tan\beta$.

Similarly, for the decay modes of the heavy neutral Higgs bosons in the MS-2HDM, the $t\bar{t}$ ($b\bar{b}$) channel is the dominant one for low (high) $\tan\beta$ values, whereas for the charged Higgs boson $h^{+(-)}$, the $t\bar{b}(\bar{t}b)$ mode is the dominant one for any $\tan\beta$. Thus, the heavy Higgs sector of the MS-2HDM can be effectively probed at the LHC through the final states involving third-generation quarks.

6.1. Charged Higgs Signal

The most promising channel at the LHC for the charged Higgs boson in the MS-2HDM is

$$gg \;\to\; \bar{t}bh^+ + t\bar{b}h^- \;\to\; t\bar{t}b\bar{b}\,. \tag{17}$$

Experimentally, this is a challenging mode due to large QCD backgrounds and the non-trivial event topology, involving at least four b-jets [25]. Nevertheless, a recent CMS study [33] has presented for the first time a realistic analysis of this process, in the leptonic decay mode of the W's coming from top decays:

$$gg \;\to\; h^{\pm}tb \;\to\; (\ell\nu_\ell bb)(\ell'\nu_{\ell'}b)b \tag{18}$$

(ℓ, ℓ' beings electrons or muons). Using the $\sqrt{s} = 8$ TeV LHC data, they have derived 95% CL upper limits on the production cross section $\sigma(gg \to h^{\pm}tb)$ times the branching ratio $\mathrm{BR}(h^{\pm} \to tb)$ as a function of the charged Higgs mass, as shown in Figure 6. In the same Figure, we show the corresponding predictions at $\sqrt{s} = 14$ TeV LHC in the Type-II MS-2HDM for some representative values of $\tan\beta$. The cross section predictions were obtained at leading order (LO) by implementing the 2HDM in `MadGraph5_aMC@NLO` [34] and using the `NNPDF2.3` PDF sets [35]. A comparison of these cross sections with the CMS limit suggests that the run-II phase of the LHC might be able to probe the low $\tan\beta$ region of the MS-2HDM parameter space using the process (17). Note that the production cross section $\sigma(gg \to \bar{t}bh^+)$ decreases rapidly with increasing $\tan\beta$ due to the Yukawa coupling suppression, even though $\mathrm{BR}(h^+ \to \bar{t}b)$ remains close to 100%. Therefore, this channel is only effective for low $\tan\beta$ values.

In order to make a rough estimate of the $\sqrt{s} = 14$ TeV LHC sensitivity to the charged Higgs signal (17) in the MS-2HDM, we perform a parton level simulation of the signal and background events using `MadGraph5` [34]. For the event reconstruction, we use some basic selection cuts

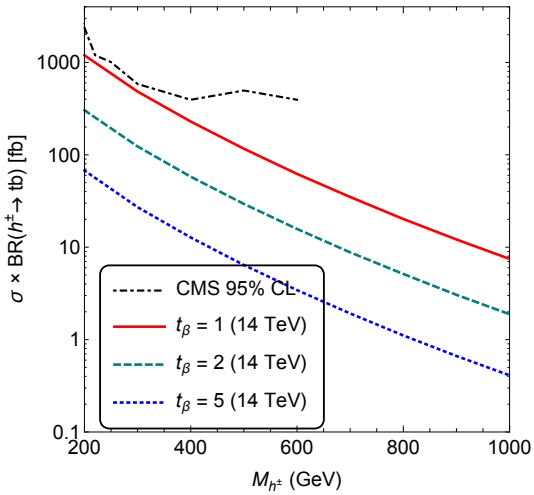

Figure 6: Predictions for the cross section of the process (17) in the Type-II MS-2HDM at $\sqrt{s} = 14$ TeV LHC for various values of $\tan\beta$. For comparison, we have also shown the current 95% CL CMS upper limit from the $\sqrt{s} = 8$ TeV data [33].

on the transverse momentum, pseudo-rapidity and dilepton invariant mass, following the CMS analysis [33]:

$$\begin{aligned} &p_T^\ell > 20 \text{ GeV}, \quad |\eta^\ell| < 2.5, \quad p_T^j > 30 \text{ GeV}, \quad |\eta^j| < 2.4, \quad \not{E}_T > 40 \text{ GeV} \\ &\Delta R^{\ell\ell} > 0.4, \quad \Delta R^{\ell j} > 0.4, \quad M_{\ell\ell} > 12 \text{ GeV}, \quad |M_{\ell\ell} - M_Z| > 10 \text{ GeV}. \end{aligned} \tag{19}$$

Jets are reconstructed using the anti-k_T clustering algorithm [26] with a distance parameter of 0.5. Since four b-jets are expected in the final state, at least two b-tagged jets are required in the signal events, and we assume the b-tagging efficiency for each of them to be 70%.

The inclusive SM cross section for $pp \to t\bar{t}b\bar{b} + X$ is ~ 18 pb at NLO, with roughly 30% uncertainty due to higher order QCD corrections [37]. Most of the QCD background for the $4b + 2\ell + \not{E}_T$ final state given by (18) can be reduced significantly by reconstructing at least one top-quark. The remaining irreducible background due to SM $t\bar{t}b\bar{b}$ production can be suppressed with respect to the signal by reconstructing the charged Higgs boson mass, once a valid signal region is defined, e.g. in terms of an observed excess of events at the LHC in future. For the semi-leptonic decay mode of top-quarks as in (18), one cannot directly use an invariant mass observable to infer $M_{h^\pm}$, as both the neutrinos in the final state give rise to missing momentum. A useful quantity in this case is the M_{T2} variable [38], defined as

$$M_{T2} = \min_{\left\{\not{\mathbf{p}}_{T_\mathrm{a}} + \not{\mathbf{p}}_{T_\mathrm{b}} = \not{\mathbf{p}}_T\right\}} \left[\max\left\{m_{T_\mathrm{a}}, m_{T_\mathrm{b}}\right\}\right], \tag{20}$$

where $\{\mathrm{a}\}, \{\mathrm{b}\}$ stand for the two sets of particles in the final state, each containing a neutrino with part of the missing transverse momentum ($\not{\mathbf{p}}_{T_{\mathrm{a,b}}}$). Minimization over all possible sums of these two momenta gives the observed missing transverse momentum $\not{\mathbf{p}}_T$, whose magnitude is the same as $\not{E}_T$ in our specific case. In (20), m_{T_i} (with i =a,b) is the usual transverse mass variable for the system $\{i\}$, defined as

$$m_{T_i}^2 = \left(\sum_{\text{visible}} E_{T_i} + \not{E}_{T_i}\right)^2 - \left(\sum_{\text{visible}} \mathbf{p}_{T_i} + \not{\mathbf{p}}_{T_i}\right)^2. \tag{21}$$

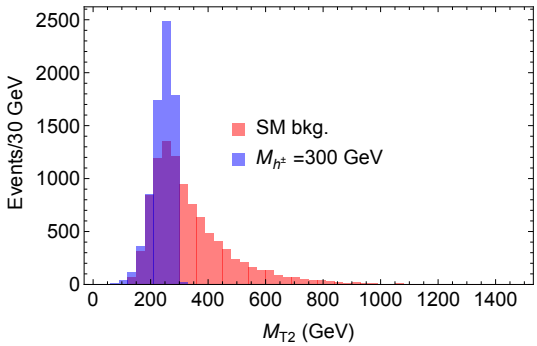

Figure 7: An illustration of the charged Higgs boson mass reconstruction using the M_{T2} variable. The irreducible SM background distribution is also shown for comparison.

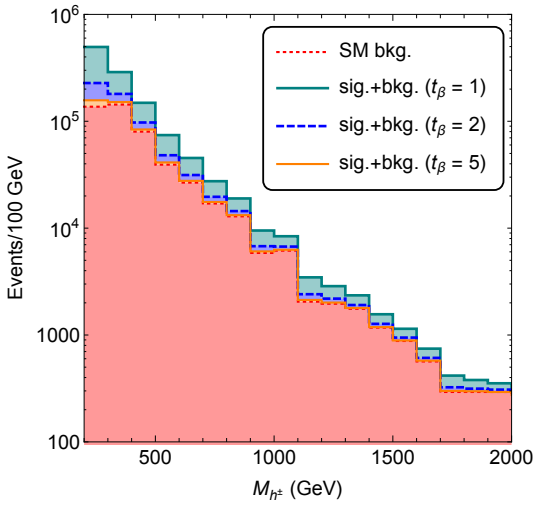

Figure 8: Predicted number of events for the $t\bar{t}b\bar{b}$ signal from the charged pseudo-Goldstone boson in the MS-2HDM at $\sqrt{s} = 14$ TeV LHC with 300 fb^{-1} integrated luminosity. The irreducible SM background (red shaded) is controlled by assuming an efficient mass reconstruction technique [11].

For the correct combination of the final state particles in (18), i.e. for $\{\mathrm{a}\} = (\ell\nu_\ell bb)$ and $\{\mathrm{b}\} = (\ell'\nu_{\ell'}bb)$ in (20), the maximum value of M_{T2} represents the charged Higgs boson mass, with the M_{T2} distribution smoothly dropping to zero at this point. This is illustrated in Figure 7 for a typical choice of $M_{h^\pm} = 300$ GeV. For comparison, we also show the M_{T2} distribution for the SM background, which obviously does not have a sharp endpoint. Thus, for a given hypothesized signal region defined in terms of an excess due to $M_{h^\pm}$, we may impose an additional cut on $M_{T2} \leq M_{h^\pm}$ to enhance the signal (18) over the irreducible SM background.

Assuming that the charged Higgs boson mass can be reconstructed efficiently, we present an estimate of the signal to background ratio for the charged Higgs signal given by (17) at $\sqrt{s} = 14$ TeV LHC with 300 fb^{-1} for some typical values of $\tan\beta$ in Figure 8. Since the mass of the charged Higgs boson is a priori unknown, we vary the charged Higgs mass, and for each value of $M_{h^\pm}$, we assume that it can be reconstructed around its actual value within 30 GeV uncertainty.

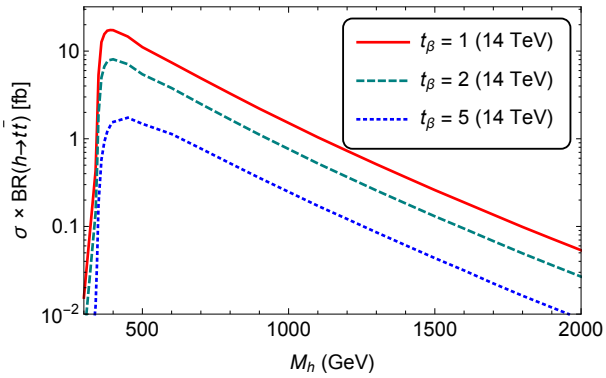

Figure 9: Predictions for the cross section of the process (22) in the Type-II MS-2HDM at $\sqrt{s} = 14$ TeV LHC for various values of $\tan\beta$.

6.2. Heavy Neutral Higgs Signal

So far there have been no direct searches for heavy neutral Higgs bosons involving $t\bar{t}$ and/or $b\bar{b}$ final states, mainly due to the challenges associated with uncertainties in the jet energy scales and the combinatorics arising from complicated multiparticle final states in a busy QCD environment. Nevertheless, these channels become pronounced in the MS-2HDM scenario, and hence, we have made a preliminary attempt to study them in [11] (see also [27]). In particular, we focus on the search channel

$$gg \;\to\; t\bar{t}h \;\to\; t\bar{t}t\bar{t}\,. \tag{22}$$

Such four top final states have been proposed before in the context of other exotic searches at the LHC (see e.g. [28]). However, their relevance for heavy Higgs searches have not been explored so far. We note here that the existing 95% CL experimental upper limit on the four top production cross section is 59 fb from ATLAS [29] and 32 fb from CMS [40], whereas the SM prediction for the inclusive cross section of the process $pp \to t\bar{t}t\bar{t} + X$ is about 10-15 fb [41].

To get a rough estimate of the signal to background ratio for our four-top signal (22), we perform a parton-level simulation of the signal and background events at LO in QCD using `MadGraph5_aMC@NLO` [34] with `NNPDF2.3` PDF sets [35]. For the inclusive SM cross section for the four-top final state at $\sqrt{s} = 14$ TeV LHC, we obtain 11.85 fb, whereas our proposed four-top signal cross sections are found to be comparable or smaller depending on M_h and $\tan\beta$, as shown in Figure 9. However, since we expect one of the $t\bar{t}$ pairs coming from an on-shell h decay to have an invariant mass around M_h, we can use this information to significantly boost the signal over the irreducible SM background. Note that all the predicted cross sections shown in Figure 9 are well below the current experimental upper bound [40].

Depending on the W decay mode from $t \to Wb$, there are 35 final states for four top decays. According to a recent ATLAS analysis [42], the experimentally favoured channel is the semi-leptonic/hadronic final state with two same-sign isolated leptons. Although the branching fraction for this topology (4.19%) is smaller than most of the other channels, the presence of two same-sign leptons in the final state allows us to reduce the large QCD background substantially, including that due to the SM production of $t\bar{t}b\bar{b}$+jets [42]. Therefore, we will only consider the following decay chain in our preliminary analysis:

$$gg \;\to\; t\bar{t}h \;\to\; (t\bar{t})(t\bar{t}) \;\to\; \Big((\ell^{\pm}\nu_\ell b)(jjb)\Big)\Big((\ell'^{\pm}\nu_{\ell'} b)(jjb)\Big)\,. \tag{23}$$

For event reconstruction, we will use the same selection cuts as in (19), and in addition, following [42], we require the scalar sum of the p_T of all leptons and jets (defined as H_T) to exceed 350 GeV.

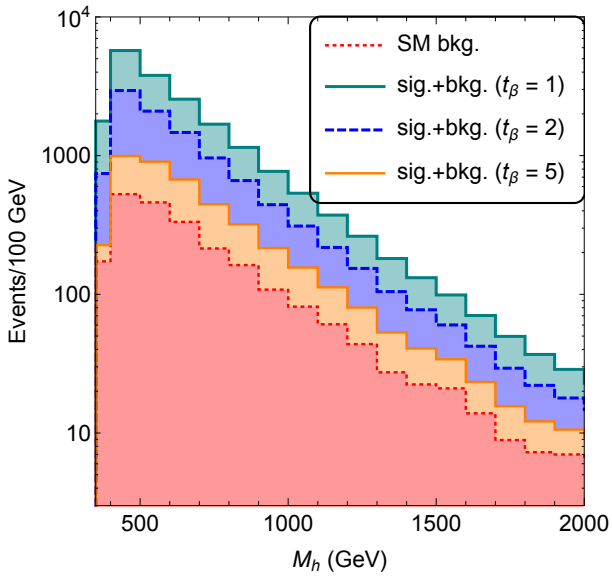

Figure 10: Predicted number of events for the $t\bar{t}t\bar{t}$ signal from the neutral pseudo-Goldstone boson in the MS-2HDM at $\sqrt{s}$ = 14 TeV LHC with 300 fb^{-1} integrated luminosity. The results are shown for three different values of $\tan\beta$ =1 (green solid), 2 (blue dashed) and 5 (orange solid). The SM background (red dotted) is controlled by assuming an efficient mass reconstruction technique, as outlined in the text.

As in the charged Higgs boson case (cf. Figure 7), the heavy Higgs mass can be reconstructed from the signal given by (23) using the M_{T2} endpoint technique, and therefore, an additional selection cut on $M_{T2} \leq M_h$ can be used to enhance the signal over the irreducible background. Our simulation results for the predicted number of signal and background events for the process (23) at $\sqrt{s} = 14$ TeV LHC with 300 fb^{-1} luminosity are shown in Figure 10. The signal events are shown for three representative values of $\tan\beta$. Here we vary the a priori unknown heavy Higgs mass, and for each value of M_h, we assume that it can be reconstructed around its actual value within 30 GeV uncertainty. From this preliminary analysis, we find that the $t\bar{t}t\bar{t}$ channel provides the most promising collider signal to probe the heavy Higgs sector in the MS-2HDM at low values of $\tan\beta \lesssim 5$.

The above analysis is also applicable for the CP-odd Higgs boson a, which has similar production cross sections and $t\bar{t}$ branching fractions as the CP-even Higgs h. However, the $t\bar{t}h(a)$ production cross section as well as the $h(a) \to t\bar{t}$ branching ratio decreases with increasing $\tan\beta$. This is due to the fact that the $ht\bar{t}$ coupling in the alignment limit is $\cos\alpha/\sin\beta \sim \cot\beta$, which is same as the $at\bar{t}$ coupling. Thus, the high $\tan\beta$ region of the MS-2HDM cannot be searched via the $t\bar{t}t\bar{t}$ channel proposed above, and one needs to consider the channels involving down-sector Yukawa couplings, e.g. $b\bar{b}b\bar{b}$ and $b\bar{b}\tau^+\tau^-$ [25]. It is also worth commenting here that the simpler process $pp \to h/a \to t\bar{t}$ ($b\bar{b}$) at low (high) $\tan\beta$ suffers from a huge SM $t\bar{t}$ ($b\bar{b}$) QCD background, even after imposing an $M_{t\bar{t}\ (b\bar{b})}$ cut. Some parton-level studies of this signal in the context of MSSM have been performed in [43].

We should clarify that the results obtained in this section are valid only at the parton level. In a realistic detector environment, the sharp features of the signal [see e.g., Figure 7] used to derive the sensitivity reach in Figures 8 and 10 may not survive, and therefore, the signal-to-background ratio might get somewhat reduced than that shown here. A detailed detector-level analysis of these signals, including realistic top reconstruction efficiencies and smearing effects, as well as possible interference effects between the charged and neutral Higgs signals and with

the SM background, is currently being pursued in a separate dedicated study [44].

7. Conclusions

We provide a symmetry justification of the so-called SM alignment limit, independently of the heavy Higgs spectrum and the value of $\tan\beta$ in the 2HDM. We show that in the Type-II 2HDM, there exist *only* three different symmetry realizations, which could lead to the SM alignment by satisfying the natural alignment condition (10) for *any* value of $\tan\beta$. In the context of the Maximally Symmetric 2HDM based on the SO(5) group, we demonstrate how small deviations from this alignment limit are naturally induced by RG effects due to the hypercharge gauge coupling g' and third generation Yukawa couplings, which also break the custodial symmetry of the theory. In addition, a non-zero soft SO(5)-breaking mass parameter is required to yield a viable Higgs spectrum consistent with the existing experimental constraints. Employing the current Higgs signal strength data from the LHC, which disfavour large deviations from the alignment limit, we derive important constraints on the 2HDM parameter space. In particular, we predict lower limits on the heavy Higgs spectrum, which prevail the present global fit limits in a wide range of parameter space. Depending on the scale where the maximal symmetry could be realized in nature, we also obtain an upper limit on the heavy Higgs masses in certain cases, which could be probed during the run-II phase of the LHC. Finally, we have studied the collider signatures of the heavy Higgs sector in the alignment limit beyond the top-quark threshold. We find that the final states involving third-generation quark final states can become a valuable observational tool to directly probe the heavy Higgs sector of the 2HDM in the alignment limit for low values of $\tan\beta$.

Acknowledgements

This work was supported by the Lancaster-Manchester-Sheffield Consortium for Fundamental Physics under STFC grant ST/L000520/1. P.S.B.D. would like to acknowledge the local hospitality provided by the CFTP and IST, Lisbon where part of these proceedings was written.

References

[1] G. Aad *et al.* [ATLAS Collaboration], Phys. Lett. B **716**, 1 (2012); S. Chatrchyan *et al.* [CMS Collaboration], Phys. Lett. B **716**, 30 (2012).
[2] P. W. Higgs, Phys. Rev. Lett. **13**, 508 (1964); F. Englert and R. Brout, Phys. Rev. Lett. **13**, 321 (1964); G. S. Guralnik, C. R. Hagen and T. W. B. Kibble, Phys. Rev. Lett. **13**, 585 (1964).
[3] G. Aad *et al.* [ATLAS and CMS Collaborations], JHEP **1608**, 045 (2016).
[4] G. C. Branco *et al.*, Phys. Rept. **516**, 1 (2012); I. P. Ivanov, arXiv:1702.03776 [hep-ph].
[5] R. A. Battye, G. D. Brawn and A. Pilaftsis, JHEP **1108**, 020 (2011).
[6] ATLAS collaboration, ATLAS-CONF-2014-010; V. Khachatryan *et al.* [CMS Collaboration], Phys. Rev. D **90**, 112013 (2014).
[7] A. Celis, V. Ilisie and A. Pich, JHEP **1307**, 053 (2013); C. W. Chiang and K. Yagyu, JHEP **1307**, 160 (2013); C.-Y. Chen, S. Dawson and M. Sher, Phys. Rev. D **88**, 015018 (2013); N. Craig, J. Galloway and S. Thomas, arXiv:1305.2424 [hep-ph]; K. Cheung, J. S. Lee and P.-Y. Tseng, JHEP **1401**, 085 (2014); L. Wang and X.-F. Han, JHEP **1411**, 085 (2014); B. Dumont, J. F. Gunion, Y. Jiang and S. Kraml, Phys. Rev. D **90**, 035021 (2014); S. Kanemura, K. Tsumura, K. Yagyu and H. Yokoya, Phys. Rev. D **90**, 075001 (2014); B. Grinstein and P. Uttayarat, JHEP **1306**, 094 (2013) [Erratum-ibid. **1309**, 110 (2013)]; A. Broggio, E. J. Chun, M. Passera, K. M. Patel and S. K. Vempati, JHEP **1411**, 058 (2014); N. Craig, F. D'Eramo, P. Draper, S. Thomas and H. Zhang, JHEP **1506**, 137 (2015); D. Chowdhury and O. Eberhardt, JHEP **1511**, 052 (2015); X. F. Han and L. Wang, arXiv:1701.02678 [hep-ph].
[8] H. Georgi and D. V. Nanopoulos, Phys. Lett. B **82**, 95 (1979).
[9] J. F. Gunion and H. E. Haber, Phys. Rev. D **67**, 075019 (2003).
[10] M. Carena, I. Low, N. R. Shah and C. E. M. Wagner, JHEP **1404**, 015 (2014); M. Carena, H. E. Haber, I. Low, N. R. Shah and C. E. M. Wagner, Phys. Rev. D **91**, 035003 (2015).
[11] P. S. B. Dev and A. Pilaftsis, JHEP **1412**, 024 (2014).

[12] D. Das and I. Saha, Phys. Rev. D **91**, 095024 (2015); J. Bernon, J. F. Gunion, H. E. Haber, Y. Jiang and S. Kraml, Phys. Rev. D **92**, 075004 (2015); H. E. Haber and O. Stål, Eur. Phys. J. C **75**, no. 10, 491 (2015).
[13] P. H. Chankowski, T. Farris, B. Grzadkowski, J. F. Gunion, J. Kalinowski and M. Krawczyk, Phys. Lett. B **496**, 195 (2000); I. F. Ginzburg and M. Krawczyk, Phys. Rev. D **72**, 115013 (2005); A. Delgado, G. Nardini and M. Quiros, JHEP **1307**, 054 (2013); G. Bhattacharyya and D. Das, Phys. Rev. D **91**, 015005 (2015).
[14] H. E. Haber and R. Hempfling, Phys. Rev. D **48**, 4280 (1993); A. Pilaftsis and C. E. M. Wagner, Nucl. Phys. B **553**, 3 (1999).
[15] M. Maniatis, A. von Manteuffel, O. Nachtmann and F. Nagel, Eur. Phys. J. C **48**, 805 (2006); C. C. Nishi, Phys. Rev. D **74**, 036003 (2006) [Erratum *ibid.* **76**, 119901 (2007)].
[16] C. C. Nishi, Phys. Rev. D **83**, 095005 (2011).
[17] A. Pilaftsis, Phys. Lett. B **706**, 465 (2012).
[18] M. Maniatis, A. von Manteuffel and O. Nachtmann, Eur. Phys. J. C **57**, 719 (2008). I. P. Ivanov, Phys. Rev. D **77**, 015017 (2008); C. C. Nishi, Phys. Rev. D **77**, 055009 (2008).
[19] J. F. Gunion and H. E. Haber, Phys. Rev. D **72**, 095002 (2005); M. Maniatis and O. Nachtmann, JHEP **1111**, 151 (2011).
[20] N. G. Deshpande and E. Ma, Phys. Rev. D **18**, 2574 (1978).
[21] R. Barbieri, L. J. Hall and V. S. Rychkov, Phys. Rev. D **74**, 015007 (2006).
[22] A. Pilaftsis, Phys. Rev. D **93**, no. 7, 075012 (2016).
[23] P. S. B. Dev and A. Pilaftsis, J. Phys. Conf. Ser. **631**, no. 1, 012030 (2015); PoS PLANCK **2015**, 105 (2015).
[24] N. Chakrabarty, P. S. B. Dev, B. Mukhopadhyaya and A. Pilaftsis, *in preparation.*
[25] D. de Florian *et al.* [LHC Higgs Cross Section Working Group], arXiv:1610.07922 [hep-ph].
[26] M. Cacciari, G. P. Salam and G. Soyez, JHEP **0804**, 063 (2008).
[27] S. Gori, I. W. Kim, N. R. Shah and K. M. Zurek, Phys. Rev. D **93**, no. 7, 075038 (2016).
[28] M. Spira and J. D. Wells, Nucl. Phys. B **523**, 3 (1998); A. Pomarol and J. Serra, Phys. Rev. D **78**, 074026 (2008); K. Kumar, T. M. P. Tait and R. Vega-Morales, JHEP **0905**, 022 (2009); S. Jung and J. D. Wells, JHEP **1011**, 001 (2010); G. L. Kane, E. Kuflik, R. Lu and L. T. Wang, Phys. Rev. D **84**, 095004 (2011); G. Cacciapaglia, R. Chierici, A. Deandrea, L. Panizzi, S. Perries and S. Tosi, JHEP **1110**, 042 (2011); E. Alvarez, D. A. Faroughy, J. F. Kamenik, R. Morales and A. Szynkman, Nucl. Phys. B **915**, 19 (2017).
[29] ATLAS Collaboration, ATLAS-CONF-2013-051.
[30] C. Patrignani *et al.* [Particle Data Group], Chin. Phys. C **40**, no. 10, 100001 (2016).
[31] R. D. Peccei and H. R. Quinn, Phys. Rev. Lett. **38**, 1440 (1977).
[32] O. Eberhardt, U. Nierste and M. Wiebusch, JHEP **1307**, 118 (2013); J. Baglio, O. Eberhardt, U. Nierste and M. Wiebusch, Phys. Rev. D **90**, 015008 (2014).
[33] CMS Collaboration, CMS-PAS-HIG-13-026.
[34] J. Alwall *et al.*, JHEP **1407**, 079 (2014).
[35] R. D. Ball *et al.*, Nucl. Phys. B **867**, 244 (2013).
[36] N. Craig, F. D'Eramo, P. Draper, S. Thomas and H. Zhang, JHEP **1506**, 137 (2015).
[37] G. Bevilacqua, M. Czakon, C. G. Papadopoulos, R. Pittau and M. Worek, JHEP **0909**, 109 (2009); M. Flechl, R. Klees, M. Kramer, M. Spira and M. Ubiali, Phys. Rev. D **91**, 075015 (2015).
[38] C. G. Lester and D. J. Summers, Phys. Lett. B **463**, 99 (1999).
[39] S. Kanemura, H. Yokoya and Y. J. Zheng, Nucl. Phys. B **898**, 286 (2015); Y. P. Kuang and L. H. Xia, Phys. Lett. B **747**, 193 (2015); N. Chen, J. Li and Y. Liu, arXiv:1509.03848 [hep-ph].
[40] V. Khachatryan *et al.* [CMS Collaboration], JHEP **1411**, 154 (2014); G. Aad *et al.* [ATLAS Collaboration], JHEP **1508**, 105 (2015).
[41] G. Bevilacqua and M. Worek, JHEP **1207**, 111 (2012).
[42] D. Paredes [ATLAS Collaboration], PhD Thesis, Université Blaise Pascal (2013), CERN-THESIS-2013-202; J. Keaveney [CMS Collaboration], arXiv:1412.4641 [hep-ex].
[43] S. Moretti and D. A. Ross, Phys. Lett. B **712**, 245 (2012); A. Djouadi, L. Maiani, A. Polosa, J. Quevillon and V. Riquer, JHEP **1506**, 168 (2015); B. Bhattacherjee, A. Chakraborty and A. Choudhury, Phys. Rev. D **92**, no. 9, 093007 (2015); M. Carena and Z. Liu, JHEP **1611**, 159 (2016).
[44] A. Choudhury, P. S. B. Dev, W. Klemm, E. Orgill, Y. Peters, A. Pilaftsis, *work in progress.*